Aerospace Science and Technology 104 (2020) 106019

Contents lists available at ScienceDirect

Aerospace Science and Technology

www.elsevier.com/locate/aescte

# Influence of viscous boundary layer on initiation zone structure of two-dimensional oblique detonation wave

Guanxiao Li, Guoqing Zhang *, Yuhang Zhang, Lucheng Ji, Shaofei Gao

*Key Laboratory of Dynamics and Control of Flight Vehicle, School of Aerospace Engineering, Beijing Institute of Technology, Beijing 100081, China*

ARTICLE INFO

*Article history:*
Received 5 August 2019
Received in revised form 15 January 2020
Accepted 8 June 2020
Available online 16 June 2020
Communicated by Craig Johansen

*Keywords:*
Viscous boundary layer
Oblique detonation
Shock wave
Chemical reaction

ABSTRACT

The influence of the viscous boundary layer on the oblique detonation wave structure has been simulated and analyzed by solving the two-dimensional Navier–Stokes equations containing the hydrogen/air elementary reaction model. It is found that the effect of the viscous boundary layer can be neglected in the smooth transition initiation structure, but not in the abrupt transition initiation structure. The interaction of the lateral shock wave and the viscous boundary layer results in the formation of a high-temperature recirculation zone near the wall of the initiation zone, a novel structure that does not appear in inviscid formulations. Within this structure, the chemical reaction is triggered to occur in advance, eventually leading to the equilibrium initiation position relocating upstream compared with the inviscid case. Nevertheless, the viscous boundary layer has a limited impact on the main flow region downstream of the oblique detonation. The shock wave structures and pressure distributions at various Mach numbers are obtained computationally and analyzed in detail.



## 1. Introduction

Both deflagration and detonation may appear in combustible reactants, but the detonation wave [1,2] is essentially different from that of deflagration. The deflagration wave has a continuous velocity spectrum, and has been widely used in conventional scramjet engines [3–5]. In contrast, the detonation wave is a relatively rare and special combustion mode [6,7]. It can be viewed as a shock wave that propagates at a supersonic velocity accompanied by a chemical reaction, achieving self-ignition of the reactant through pre-excited shock compression. Generally speaking, detonation is an approximately isovolumetric combustion process; it has a higher thermodynamic cycle efficiency, and can therefore be used in aeronautic and astronautic engines [8–13].

Oblique detonation engines are a form of detonation-based ramjet that have great application potential in the propulsion system of hypersonic vehicles [14–19]. The structure of oblique detonation was first reported by Li et al. [20] following numerical simulations, and was later verified and discussed by Viguier et al. [21]. Broda [22] found a different type of detonation structure through a series of experiments. This structure did not have a mutation pattern similar to a three-wave point structure, but a smooth wave surface structure. Vlasenko & Sabelnikov [23] confirmed the existence of the oblique detonation wave (ODW) of this smooth detonation structure through numerical simulations. Since then, the detonation area of the ODW has been divided into two transitional forms: abrupt and smooth. In recent years, numerous studies have attempted to clarify the structure of the initiation region, which concerns the interaction of the oblique shock, deflagration, compression wave, and other components [24–32]. The instability of the oblique detonation surface has been investigated, indicating the formation of local fine wave structures [33–40]. Furthermore, to advance engine applications, new numerical algorithms [41–45] have been developed and effects such as inflow unsteadiness and inhomogeneity have been studied to deepen our understanding of the oblique detonation dynamics [46–53].

Although oblique detonations have been extensively studied, the effect of viscosity has often been ignored. This is because the viscosity has little effect on the oblique detonation after the oblique shock wave [20,54,55]. In normal detonation research, the effect of viscosity is often ignored [56,57], because the interaction of the shock and the heat release is thought to dominate the flow. However, a recent study [58] demonstrated that diffusion and hydrodynamic instabilities may play a key role in unstable detonations. As the research in this field becomes deeper, it is necessary to look at whether the viscous effects of oblique detonation can be neglected in all circumstances. When the oblique shock wave is transformed into the detonation wave, two transition patterns are observed: smooth transition and abrupt transition [23,26]. This study focuses on how these two detonation wave structures in-

* Corresponding author.
*E-mail address:* zhanggq@bit.edu.cn (G. Zhang).

https://doi.org/10.1016/j.ast.2020.106019
1270-9638/

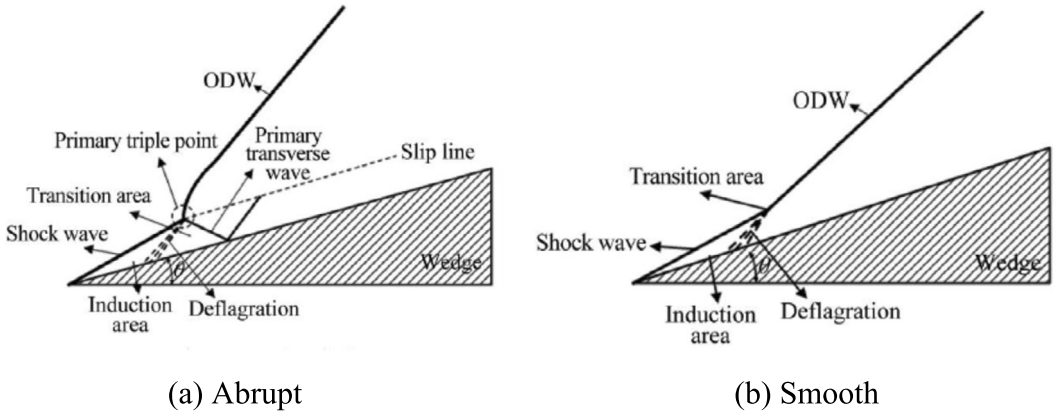


**Fig. 1.** Transition mode detonation zone structure [23].

teract with the viscous boundary layer, and whether the inviscid detonation structure is fundamentally altered as a result.

## 2. Simulation methods

As the present research involves both inviscid and viscous turbulent flow field simulations, the governing equations are multi-component Navier–Stokes equations for additional chemical reaction source terms based on the finite volume method. In preliminary calculations considering the boundary layer, the turbulence is not included so that the primary effect, i.e., the influence of the viscous boundary layer, can be highlighted. Undoubtedly, the boundary layer will become turbulent downstream, but a qualitative study based on the assumption of laminar flow should be sufficient to capture the main wave structures, providing a foundation for future work on the effects of turbulence. The equations governing a two-dimensional compressible laminar flow multi-component finite-rate chemical reaction gas can be written as:

$$\frac{\partial U}{\partial t}+\frac{\partial F}{\partial x}+\frac{\partial G}{\partial y}=\frac{\partial F_v}{\partial x}+\frac{\partial G_v}{\partial y}+S \tag{1}$$

$$U=\begin{bmatrix}\rho\\ \rho u\\ \rho v\\ E\\ \rho Y_1\\ \cdots\\ \rho Y_{NS-1}\end{bmatrix},\quad F=\begin{bmatrix}\rho u\\ \rho u^2+p\\ \rho uv\\ (E+p)u\\ \rho uY_1\\ \cdots\\ \rho uY_{NS-1}\end{bmatrix},\quad G=\begin{bmatrix}\rho v\\ \rho uv\\ \rho v^2+p\\ (E+p)v\\ \rho vY_1\\ \cdots\\ \rho vY_{NS-1}\end{bmatrix},$$

$$F_v=\begin{bmatrix}0\\ \tau_{xx}\\ \tau_{xy}\\ u\tau_{xx}+v\tau_{xy}+q_x\\ \rho D_{1,m}(Y_1)_x\\ \cdots\\ \rho D_{NS-1,m}(Y_{NS-1})_x\end{bmatrix},$$

$$G_v=\begin{bmatrix}0\\ \tau_{xy}\\ \tau_{yy}\\ u\tau_{xy}+v\tau_{yy}+q_y\\ \rho D_{1,m}(Y_1)_y\\ \cdots\\ \rho D_{NS-1,m}(Y_{NS-1})_y\end{bmatrix},\quad S=\begin{bmatrix}0\\ 0\\ 0\\ 0\\ 0\\ \dot{\omega}_1\\ \cdots\\ \dot{\omega}_{NS-1}\end{bmatrix} \tag{2}$$

In equation (2), $\rho$ and $p$ are the density and pressure of the mixture; $u$ and $v$ denote the velocity in the $x$ and $y$ directions, respectively. $E$ is the total energy per unit volume, defined as:

$$E=\rho h-p+\frac{1}{2}\rho\left(u^2+v^2\right) \tag{3}$$

For multi-component combustible gases, NS is the number of components, $Y_i$ is the mass fraction of the $i$th component, and the sum of the mass fractions of each component is 1. $D_{i,m}$ and $\dot{\omega}_i$ are the mass diffusion coefficients and mass generation rate of the $i$th component, respectively.

The shear stress $\tau$ and heat flux $q$ in the viscous term are written as:

$$\begin{cases}\tau_{xx}=2\mu u_x-\frac{2}{3}\mu(u_x+v_y)\\ \tau_{xy}=2\mu v_y-\frac{2}{3}\mu(u_x+v_y)\\ \tau_{xy}=\tau_{yx}=\mu(u_y+v_x)\end{cases}$$

$$\begin{cases}q_x=kT_x+\rho\sum_{i=1}^{NS}h_iD_{i,m}(Y_i)_x\\ q_y=kT_y+\rho\sum_{i=1}^{NS}h_iD_{i,m}(Y_i)_y\end{cases} \tag{4}$$

where $T$ is the temperature of the gas, $k$ is the heat transfer coefficient of the mixed gas, $h_i$ is the specific enthalpy of the $i$th component, and $\mu$ is the laminar viscosity coefficient given by Sutherland's formula. This study uses the high-pressure hydrogen–oxygen combustion kinetics elementary reaction model proposed by Burke et al. [59], involving 13 components ($H_2$, $O_2$, O, H, OH, $HO_2$, $H_2O_2$, $H_2O$, $N_2$, N, NO, Ar, He) and 27 single-step reversible elementary reactions. The CHEMKIN package [60] is used to solve the chemical reactions.

The present numerical simulations are based on the density solver and the ideal gas hypothesis, and the governing equations are solved in an explicit format. The advection upstream splitting method is used to control the flux, and the second-order upwind style is adopted to discretize the convection term. The fourth-order Runge–Kutta method is used for the timing integration to guarantee temporal accuracy. Numerical simulations of the two-dimensional flow field assume the high-altitude inflow condition.

Fig. 1 shows the two types of transition mode detonation zone structure, abrupt (Fig. 1(a)) and smooth (Fig. 1(b)) [23]. As shown in Fig. 2(a), the premixed hydrogen/air flammable supersonic flow

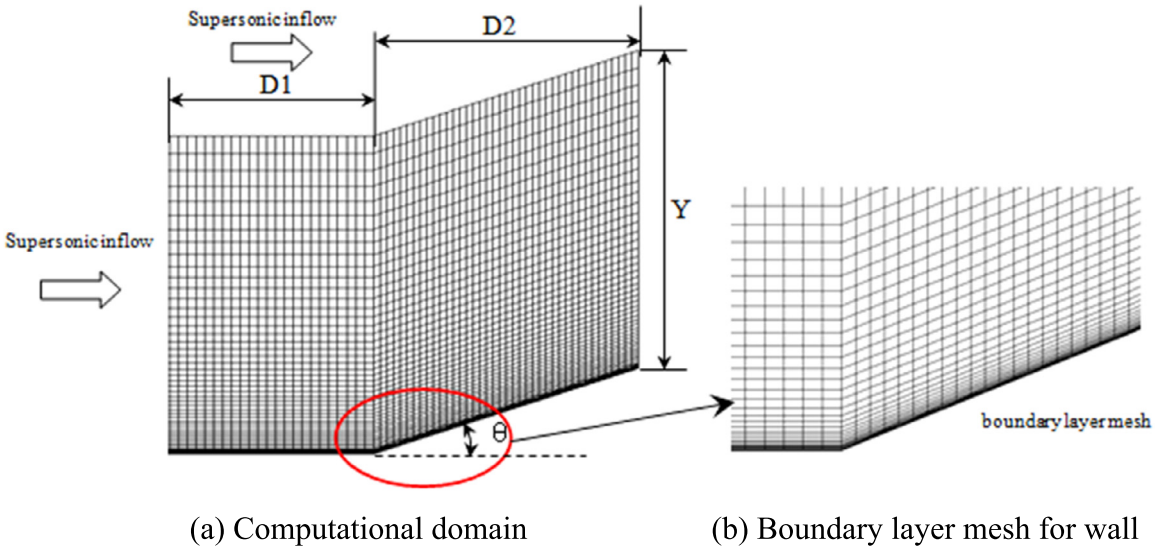


**Fig. 2.** Generation of the ODW.

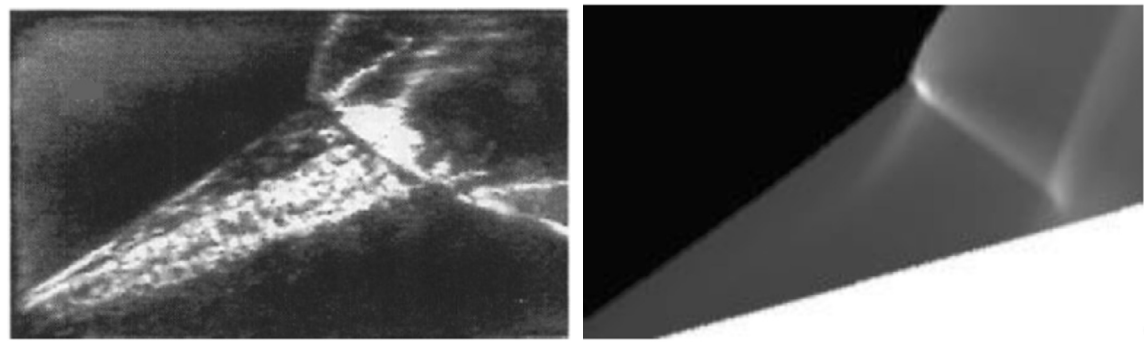


**Fig. 3.** Comparison of the experimental and simulated data.

induces an oblique shock wave through the wedge surface, and the pre-mixed gas is heated by the oblique shock wave. When the premixed gas reaches a certain temperature, an exothermic chemical reaction occurs, generating an ODW. The inlet height $Y = 90$ mm, the wedge surface starts at $D_1 = 20$ mm, the length of the wedge surface along the $x$-axis is $D_2 = 60$ mm, and the angle of the wedge surface to the horizontal plane is $\theta = 22°$. The premixed combustible gas is a mixture of $H_2$, $O_2$, and $N_2$, and the volume fraction ratio of the premixed gas is $H_2{:}O_2{:}N_2 = 2 \times ER{:}1{:}3.76$, where $ER = 0.34$ is an equivalent ratio. The initial pressure of the incoming flow is $p_0 = 63$ kPa, the initial temperature $T_0 = 872$ K, and the incoming Mach number is 2.9. These parameters correspond to a representative inflow condition that has been compressed by the oblique shock from the forebody and inlet, as used in other studies [28,29].

For both inviscid and viscous flow fields, the initial conditions prescribe uniform inflow, and the oblique shock forms because of the presence of the wall. However, the boundary conditions vary depending on whether viscosity is included. When simulating the flow field based on the inviscid flow hypothesis, a slip wall boundary is applied, that is, the velocity of the fluid at the wall position is not necessarily zero; in the case of viscous flow, a nonslip wall boundary is used, that is, the velocity of the fluid at the wall position is zero. Three boundaries, including the pre-wall, left inlet, and upper boundaries, are assumed to have supersonic inflow. The post-detonation boundaries away from the wall, including the right boundary and part of the upper boundary, are set to have supersonic outflow without the disturbance traveling upstream. As shown in Fig. 2(b), the simulation of the viscous boundary layer requires the wall mesh to be refined. After several trials, the size of the wall mesh cells is set to be 10 μm, which corresponds to about 25 grid cells in the boundary layer. The subsequent mesh is increased by a factor of 1.1 until the mesh size is the same as the set value.

To verify the accuracy of the numerical method, the simulation results were compared with experimental data reported by Viguier et al. [21]. As shown in Figs. 3(a) and 3(b), the resulting pre-mixed combustible gas at Mach 7.5 is formed under the action of a 25° wedge. The figure shows that the simulated structure of the oblique detonation zone is similar to the experimentally determined structure, demonstrating that the numerical method provides high-quality results. Furthermore, to verify the grid independence of the numerical method, numerical calculations were performed on the abovementioned numerical flow fields using two grids (corresponding to maximum grid size dimensions of 150 μm and 75 μm, respectively), and the results were compared to ensure that the grid size does not affect the numerical calculation results.

Fig. 4(a) shows a flow field diagram obtained by the 150-μm precision mesh simulation. Compared with the pressure flow field diagram shown in Fig. 4(b), as obtained by the 75-μm precision mesh simulation, it can be considered that the grid size

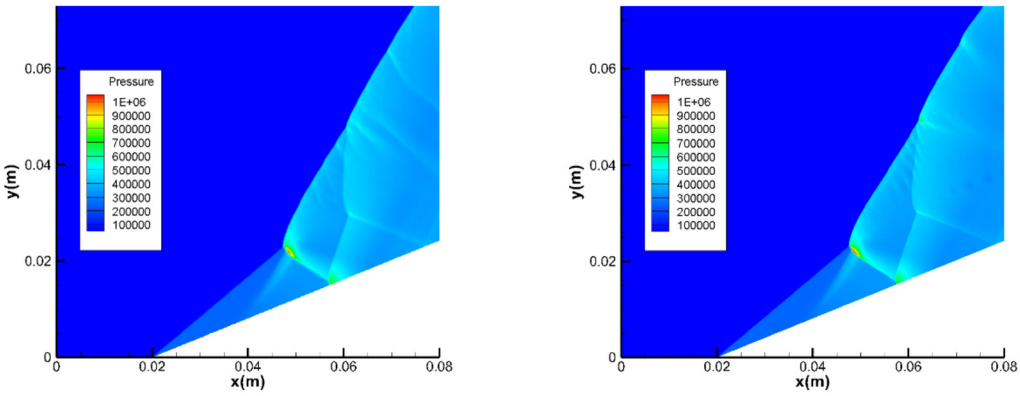


**Fig. 4.** Pressure fields of ODW using different grid sizes at Mach 2.9. Left: maximum grid size of 150 μm; right: maximum grid size of 75 μm. (For interpretation of the colors in the figure(s), the reader is referred to the web version of this article.)

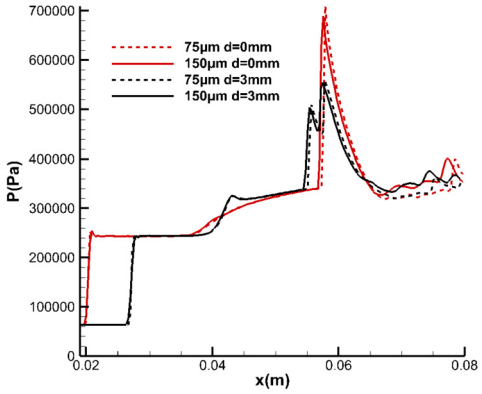


**Fig. 5.** Pressure distribution along different lines (d = 0 mm and d = 3 mm) using different grid sizes at Mach 2.9.

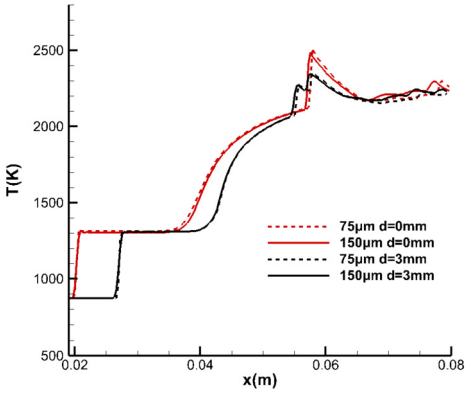


**Fig. 6.** Temperature distribution along different lines (d = 0 mm and d = 3 mm) using different grid sizes at Mach 2.9.

has little effect on the simulation results. The main wave configurations are almost the same, except for small differences in the fine structures on the unstable surface. Because the fine structures do not influence the main configuration (particularly the upstream boundary layer, which is the focus of this qualitative study), the resolution used in Fig. 4(b) was considered sufficient for the subsequent simulations. To examine the influence of grid precision on the simulation results, quantitative pressure/temperature distributions along straight lines parallel to the wall surface are plotted in Figs. 5 and 6. The distance from a straight line to the wall surface of the wedge surface is defined as $d$, e.g., when $d = 0$ mm, the line is the surface of the wedge surface. Fig. 5 shows the pressure variation along different straight lines in the flow field after a standing ODW occurs at around 0.2 μs with the different mesh sizes; Fig. 6 shows the temperature variation for the same cases. The difference between the pressure and temperature changes corresponding to different grid sizes is very small. Some local errors are generated because the ODW structure in the standing state is not completely steady, and small oscillations at different moments cause the curves to be slightly different. Thus, for the selected numerical methods and mesh precision, the validity of the simulation results and the reliability of the conclusions can be guaranteed.

## 3. Numerical results

According to the research of Teng et al. [26,27], an increase in the Mach number causes the initiation structure to change from an abrupt transition to a smooth transition. Under the premise of ensuring grid independence, the wedge-induced oblique detonation of incoming flows traveling at Mach 2.9 and 3.5 was numerically simulated in the viscous and inviscid flow fields. The temperature flow fields in the detonation zone are shown in Figs. 7 and 8. The oblique detonation initiation structure in the flow field is consistent with the process described in Section 1. In the case where the incoming Mach number is 2.9, the transition from oblique shock wave surface to ODW surface is abrupt; when the incoming Mach number is 3.5, the transition is smooth. Intuitively, for the smooth transition of the oblique detonation initiation structure, the difference between the viscous flow and the inviscid flow is only reflected in the high-temperature zone formed by the viscous boundary layer at the wall surface, and the overall structure of the flow field is not significantly different. For the abrupt transition of the oblique detonation initiation structure, under the influence of the viscous boundary layer, the flow field structure near the detonation zone changes markedly, and the location of the initiation and the length of the induction zone are significantly different.

In the abrupt transitional initiation structure of the inviscid oblique detonation flow field, chemical reactions accumulate to form deflagration waves, which then converge into detonation waves. Under the inflow condition and flow field model of this paper, the $x$-axis coordinate of the inflection point of the detonation structure (also called the three-wave point) is ∼0.047 m. Under the influence of viscosity, the position of the three-wave point obviously moves forward, and its $x$-axis coordinate reaches ∼0.036 m. Under the deflagration wave convergence area, a high-temperature zone is formed under the influence of viscosity, and a detonation wave is generated thereafter. The high-temperature zone induced by the viscous boundary layer affects the progress of the chemical reaction, which in turn causes the deflagration wave to converge faster to form a detonation wave. Additionally, for the abrupt tran-

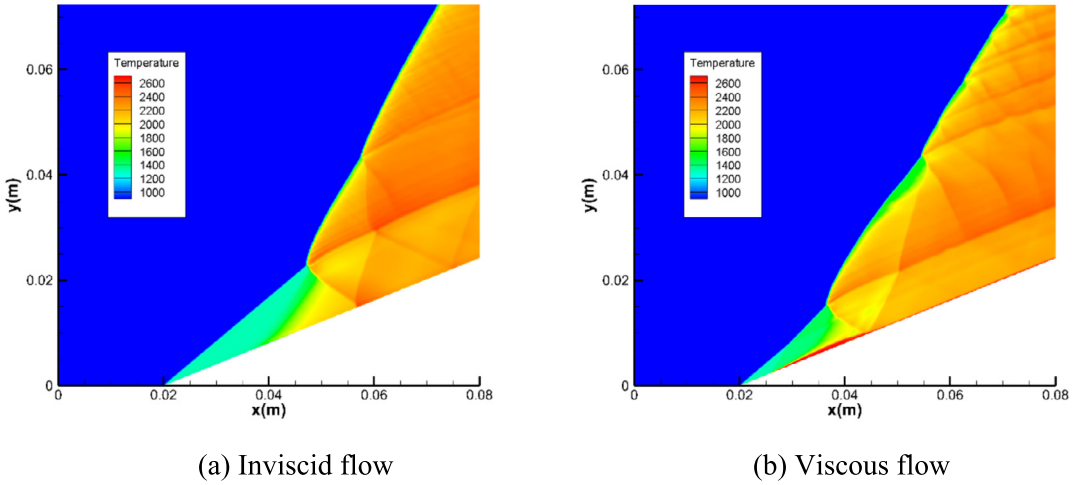


(a) Inviscid flow (b) Viscous flow

**Fig. 7.** Temperature fields in the detonation zone at Mach 2.9.

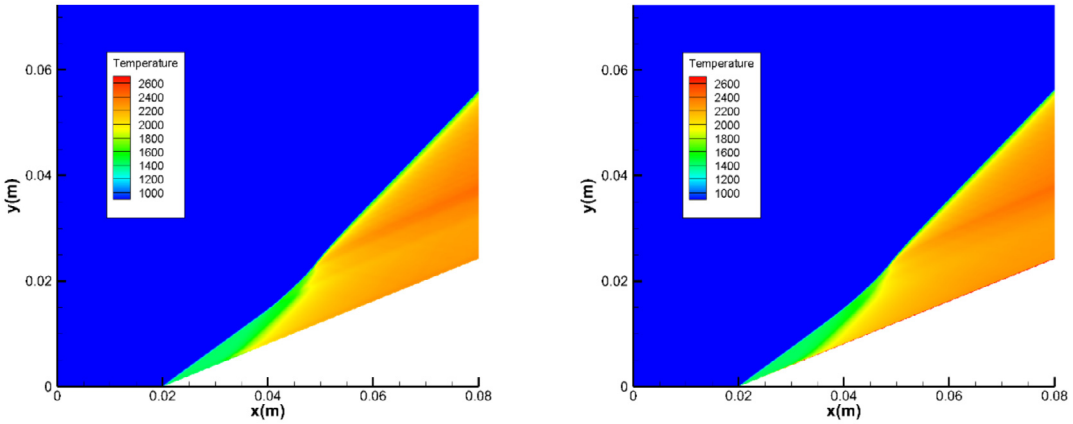


(a) Inviscid flow (b) Viscous flow

**Fig. 8.** Temperature fields in the detonation zone at Mach 3.5.

sition at Mach 2.9 (Fig. 7), there is a noticeable shock-reaction decoupling after the triple point, and the downstream ODW surface seems more irregular and partially decoupled for the viscous ODW. The decoupling actually occurs without considering viscosity, but is suppressed by the reflected oblique shock. When considering viscosity, the initiation moves upstream and the reflected shock makes a small angle with the wedge, thus interacting with the ODW surface downstream. These effects collectively generate a long smooth surface, allowing for obvious decoupling in the viscous ODW. The downstream surface is then impacted by a strong disturbance, so can easily become unstable. The shock–heat release decoupling and evolution of the small-amplitude disturbance have previously been analyzed [36], where similar phenomena as in this study were observed, despite the use of different physical and chemical models.

For comparison with the temperature field shown in Fig. 7(b), the corresponding pressure field is plotted in Fig. 9. For both inviscid and viscous flow fields, the pressure peak appears just behind the turning point of the oblique shock wave and the oblique detonation, that is, the three-wave point. Therefore, the state of the current flow field can be judged by comparing the change in the position of this point with respect to time during the initiation process. Fig. 10 compares the variation of the pressure peak position of the ODW system with time in the inviscid and viscous flow fields. In the inviscid case, the position of peak pressure in the ODW system becomes relatively stable within 0.2 ms. This indicates that the ODW reaches the standing state, and reflects the relatively simple and rapid establishment of the detonation structure in the inviscid flow field. In contrast, in the viscous flow field, the peak pressure position does not stabilize quickly after the initiation, but slowly enters a relatively stationary state under the

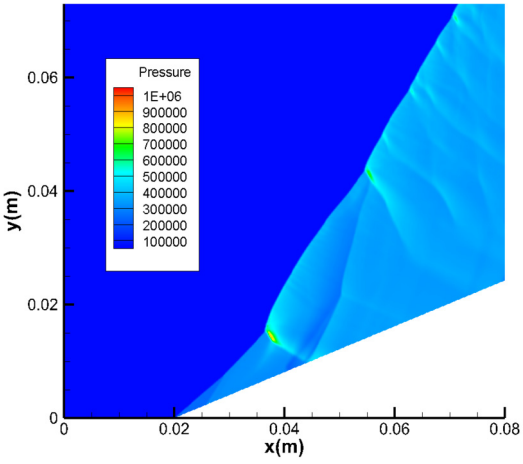


**Fig. 9.** Pressure fields under the influence of the viscous boundary layer at Mach 2.9.

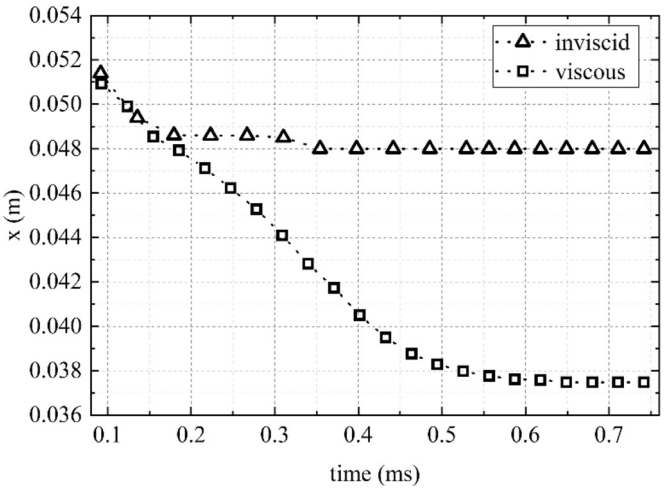


**Fig. 10.** Time-dependent changes of pressure peak $x$-axis coordinates in inviscid and viscous flow fields.

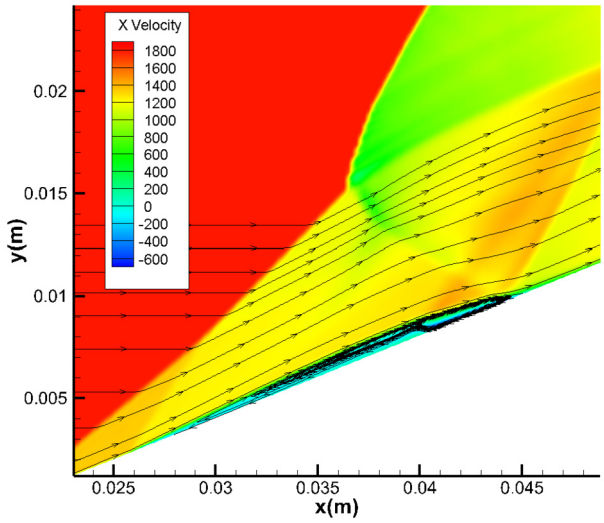


**Fig. 11.** Streamline near the initiation zone of the abrupt transition structure under the influence of the viscous boundary layer.

influence of the boundary layer. It takes much longer to establish a detonation wave standing structure in a viscous flow field than an inviscid flow field. Moreover, note that diffusion effects seem to be absent in the present numerical results, except in the boundary layer and the related recirculation zone. Considering the high Reynolds number (of order $10^6$), this is reasonable, but should be considered in future work. The following discussion continues to explore how the viscous boundary layer interferes with the establishment of the detonation structure, and thus the entire flow field.

The $x$-velocity cloud image of the high-temperature zone of the wall is enlarged, and the streamline in Fig. 11 indicates that a plurality of vortex groups (also called the separation zone or recirculation zone) forms near the wall surface of the high-temperature zone under the influence of viscosity. The appearance of these vortexes causes the upstream oblique shock wave to be further compressed compared with the inviscid flow field. In addition, the high temperature of the separation zone causes the chemical reaction to occur more quickly, resulting in the initiation position advancing. The change in the separation zone over the whole detonation process suggests that the tail of the vortex in the separation zone always intersects with the transverse wave of the induction zone,

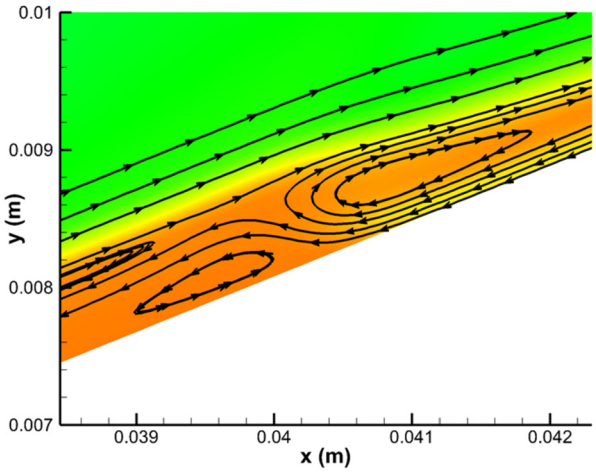


**Fig. 12.** Streamline in viscous boundary layer separation zone.

and the streamline that should flow downstream along the wall is blocked by the transverse wave to generate a vortex.

To display the local structure clearly, Fig. 12 shows the temperature with streamlines in an enlarged diagram of the recirculation zone. As well as the main vortex in the downstream region, there is a plurality of small vortex groups in the upstream area. Direct blocking by the transverse wave means that the main vortex is located at the end of the separation zone, and rotates clockwise. For the plurality of small vortex groups, the upstream vortex close to the main vortex rotates counterclockwise, while the other vortex group is rotating clockwise. The above results demonstrate that the abrupt transition structure of the oblique detonation blocks the boundary layer, which then moves downstream because of the existence of the transverse wave and interacts with the lateral shock wave, generating a recirculation zone. Once the recirculation zone has been created, it is accompanied by high temperatures and then fast chemical reactions. Thereafter, the recirculation zone moves upstream, and the length and width of the recirculation zone increase, which in turn accelerates the heat release. The interaction of this complicated wave configuration causes the initiation structure to oscillate compared with the inviscid flow field, which explains why the abrupt flow initiation structure in the viscous flow field takes longer to reach the standing state.

The process described above allows us to explain the establishment of the wave structure of the abrupt oblique detonation transition in the inviscid and viscous flow fields when the incoming Mach number is 2.9. The wall pressure and temperature of the inviscid and viscous flow fields along the wall when the incoming Mach number is 2.9 are compared in Fig. 13. For the inviscid flow field, after the premixed flow has passed through the oblique shock wave, the temperature and pressure increase abruptly, although no heat release occurs. Because the wall in the inviscid flow field is a slip wall, the gas flow is uniform without the viscous boundary layer, and the heat release begins rapidly at the end of the induction zone. The pressure and temperature in the inviscid flow field undergo a significant rise and fall, which can be attributed to the formation of a compression wave coupled with deflagration. A similar phenomenon occurs downstream, indicating that the transverse wave is reflected between the slip line and the wall. However, the flow field affected by a viscous boundary layer is much more complicated. Compared with the inviscid flow field, the kinetic energy is converted into internal energy under the influence of the nonslip wall after the pre-mixed gas flow, and the temperature increases as the velocity decreases. Hence, a violent chemical reaction occurs at an early stage, and the temperature increases sharply. There is a significant drop in temperature and

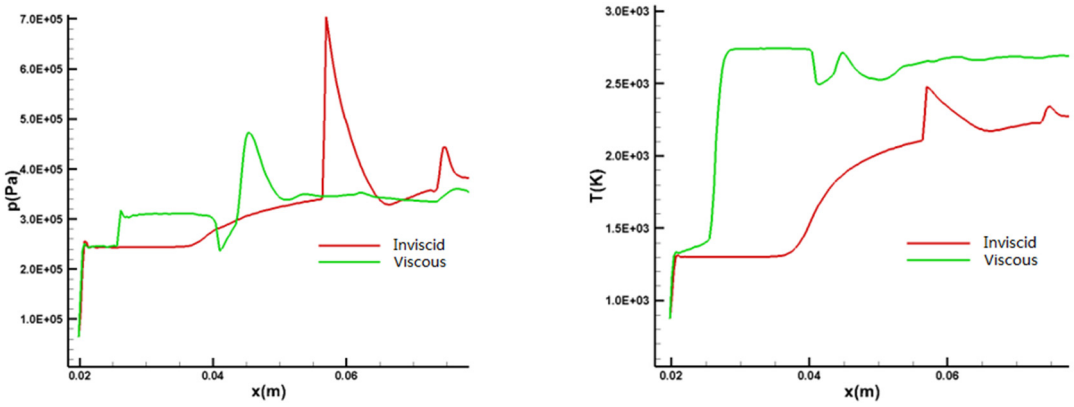


**Fig. 13.** Pressure (left) and temperature (right) along the wall for inviscid and viscous flow fields at Mach 2.9.

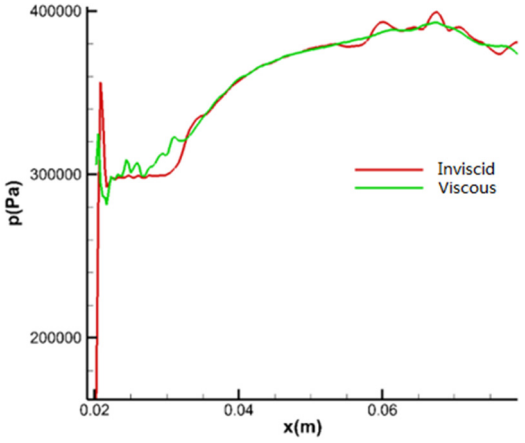


**Fig. 14.** Comparison of wall pressure between inviscid and viscous flow field at Mach 3.5.

pressure near 0.04 m, corresponding to the starting position of the main vortex in the separation zone. It is not surprising that the recurrent rises and falls in pressure and temperature are consistent with the same conditions in the inviscid flow field, as they are all manifestations of the transverse wave at the wall. This reflects the interaction between the separation zone and the transverse wave.

From the above analysis, the reason for the viscous boundary layer having a significant influence on the oblique detonation initiation structure of the abrupt transition can be determined: the interaction between the complex transverse wave structure and the boundary layer in the abrupt transition structure enhances the chemical reaction. As the smooth transition pattern does not have these complex transverse waves and three-wave structures, the viscous boundary layer shown in Fig. 8 has almost no effect on the flow field of the smooth transition pattern. The wall pressures of the inviscid and viscous flow fields in the smooth transition when the incoming Mach number is 3.5 are shown in Fig. 14. It can be seen that the trends and values are highly consistent. Regarding the transition mode, it is known that an increase in the Mach number causes the abrupt transition pattern to become a smooth transition pattern, and there is an intermediate state between them.

Fig. 15 shows the flow field structures of the oblique detonation initiation zone with incoming Mach numbers of 3.1 and 3.3 under the condition of an inviscid flow field. To a certain extent, this can be regarded as the intermediate state of the transition mode. The structure of the initiation zone is still abrupt when the Mach number is 3.1, but the transverse wave intensity is obviously weaker than the flow field structure at Mach 2.9, and the interaction of the transverse wave and the slip line on the wall has also weakened. The starting position of the chemical reaction in the induction zone moves forward, and the wavefront angle of the downstream detonation wave becomes smaller. This indicates that the overall structure is changing to a smooth transition. According to the previous definition, the structure of the initiation zone at Mach 3.3 can no longer be regarded as an abrupt transition mode. The entire transverse wave almost disappears and the slip line intensity is greatly weakened. Additionally, the three-wave point position is blurred and the downstream detonation wavefront angle is further reduced. At this point, the overall structure is similar to that of the smooth transition.

Based on the above analysis, the influence of the viscous boundary layer on the detonation structure is based on the interaction with the transverse wave structure, which has a significant effect on the abrupt transition initiation but almost no effect on the smooth transition initiation. Thus, the influence of the intermediate state on the initiation pattern depends mainly on the transverse wave intensity in the flow field. Fig. 16 shows the pressure change along the wall of the inviscid and viscous flow fields at incoming Mach numbers of 3.0, 3.1, and 3.3. The transition from Mach 3.0 to 3.3 corresponds to the detonation wave initiation structure changing from an abrupt transition to a smooth transition. It can be seen that the variation in pressure at Mach 3.0 is similar to that in Fig. 13(a)—the interaction between the transverse wave and the boundary layer is still significant, but the viscous effect is weaker than when the Mach number is 2.9. When the Mach number is 3.1, the decrease in the pressure peak represents the weakening of the shear wave intensity, and the influence of the interaction with the viscous boundary layer is further reduced. When the Mach number is 3.3, similar to Fig. 14, the pressure peak almost disappears, the transition structure changes from an abrupt transition to a smooth transition, and the pressure curve under the viscous effect is almost identical to that in the inviscid flow field.

Based on the above results, we can conclude that the viscous boundary layer largely affects the abrupt transition structure of the wedge-induced oblique detonation initiation zone. It is worth noting that, in engineering practice, the downstream band of the ODW is often more important, because most of the combustion occurs behind the detonation wavefront. As mentioned above, most research on oblique detonation has been based on the inviscid flow hypothesis: does this mean that the inviscid condition is no longer applicable? To answer this question, attention should shift from the initiation zone to the downstream detonation band, because the mainstream zone of the oblique detonation band is critical to the performance of the oblique detonation engine. Fig. 17 com-

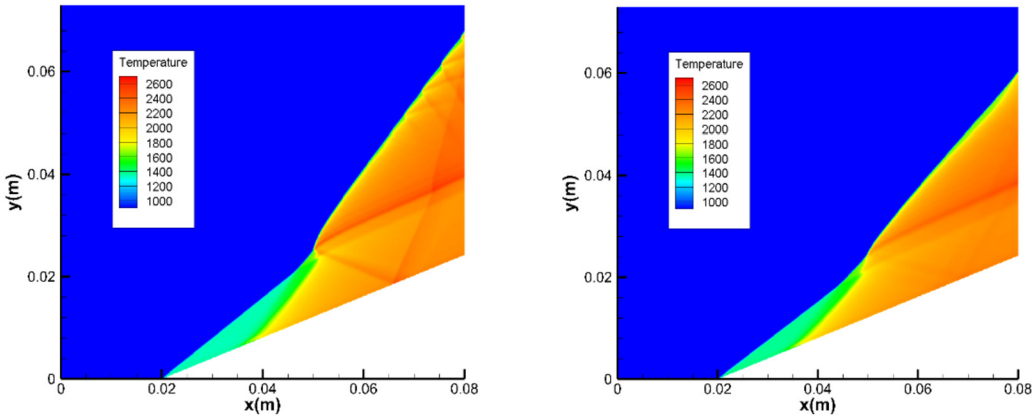


**Fig. 15.** Initiation zone structure of inviscid flow field at Mach 3.1 (left) and 3.3 (right).

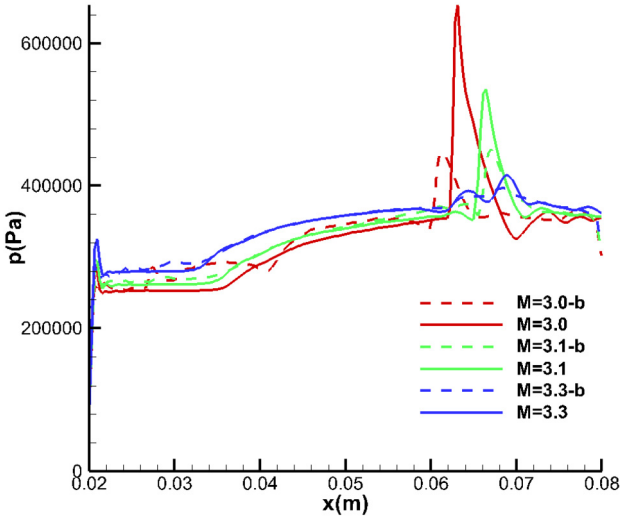


**Fig. 16.** Pressure curve along the wall of inviscid and viscous flow fields under different Mach numbers.

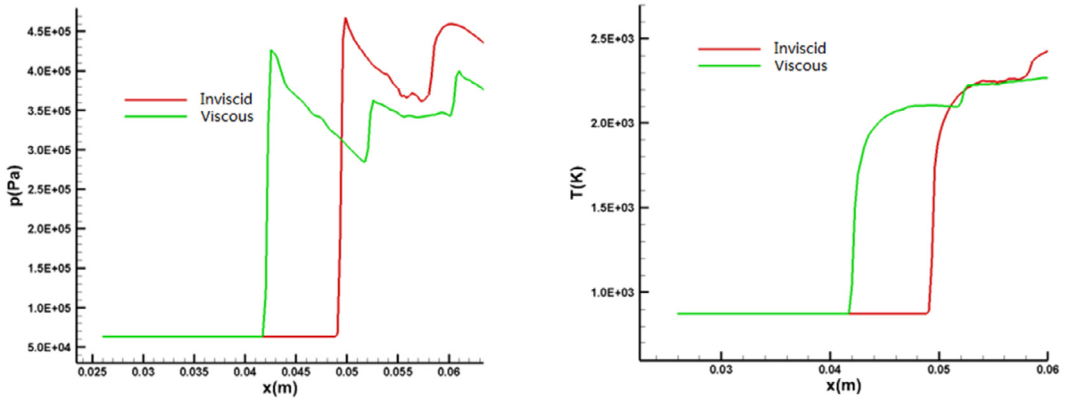


**Fig. 17.** Comparison of the oblique detonation band in inviscid and viscous flow fields at Mach 2.9.

pares the pressure (Fig. 17(a)) and temperature (Fig. 17(b)) of the inviscid and viscous flow fields in the detonation band when the incoming Mach number is 2.9. A comparison of the pressure and temperature curves of the inviscid and viscous flow fields at the wall shows that the effect of viscosity in the oblique detonation band is only reflected in the position difference, and the variation trends and magnitude of change in pressure and temperature are highly similar. Therefore, although the viscous boundary layer has a significant influence on the initiation structure of the oblique detonation and leads to the appearance of a separation zone, there is no obvious influence on the downstream detonation band. Thus, in the case of research on the performance of the downstream det-

onation band, the assumption of an inviscid flow field is still an effective technical approach.

## 4. Conclusion

(1) When the initiation is an abrupt transition structure, it will be greatly affected by the viscous boundary layer. When the initiation is a smooth transition structure, the viscous boundary layer has almost no effect on the oblique detonation structure. The key point is whether the intensity of the transverse wave in the abrupt transition structure is sufficiently large and interacts with the boundary layer.
(2) The complex transverse wave structure in the abrupt transition can block the development of the boundary layer, and a high-temperature recirculation zone containing a plurality of vortexes will appear near the wall below the induction zone. The chemical reaction is accelerated and occurs in advance under the high temperature of the recirculation zone, which can lead to the three-wave point advancing in the initiation structure. In turn, this promotes the formation of the recirculation zone.
(3) As the initiation structure changes from an abrupt transition to a smooth transition, the intensity of the transverse wave structure and its interaction with the boundary layer become weaker, and the recirculation zone will gradually disappear.
(4) When the initiation pattern changes to a smooth transition, the transverse wave will disappear and the viscous boundary layer will not affect the initiation structure. Therefore, the influence of the viscous boundary layer on the ODW structure is mainly concentrated in the initiation zone of the abrupt transition pattern.

## Declaration of competing interest

The authors declare that they have no known competing financial interests or personal relationships that could have appeared to influence the work reported in this paper.

## Acknowledgement

This research is supported by the National Key R&D Program of China [2018YFF0300800].

## References

[1] K.K. Kuo, Principles of Combustion, Wiley, 2005.
[2] C.K. Law, Combustion Physics, Cambridge Univ. Press, 2006.
[3] W.H. Heiser, D.T. Pratt, Hypersonic Airbreathing Propulsion, Am. Inst. Aeronaut. Astronaut., Washington, DC, 1994.
[4] E.T. Curran, W.H. Heiser, D.T. Pratt, Fluid phenomena in scramjet combustion systems, Annu. Rev. Fluid Mech. 28 (1996) 23–60.
[5] J. Urzay, Supersonic combustion in air-breathing propulsion systems for hypersonic flight, Annu. Rev. Fluid Mech. 50 (2018) 593–627.
[6] W. Fickett, W.C. Davis, Detonation: Theory and Experiment, Dover Publications, Courier Corporation, 2000.
[7] J.H.S. Lee, The Detonation Phenomenon, Cambridge University Press, New York, 2008.
[8] G.D. Roy, S.M. Frolov, A.A. Borisov, D.W. Netzer, Pulse detonation propulsion: challenges, current status, and future perspective, Prog. Energy Combust. Sci. 30 (2004) 545–672.
[9] E.M. Braun, F.K. Lu, D.R. Wilson, J.A. Camberos, Airbreathing rotating detonation wave engine cycle analysis, Aerosp. Sci. Technol. 27 (2013) 201–208.
[10] P. Wolanski, Detonation propulsion, Prog. Energy Combust. Sci. 34 (2013) 125–158.
[11] L. Lin, C. Weng, Q. Chen, H. Jiao, Study on the effects of ionization seeds on pulse detonation characteristics, Aerosp. Sci. Technol. 71 (2017) 128–135.
[12] Y. Wang, J. Le, A hollow combustor that intensifies rotating detonation, Aerosp. Sci. Technol. 85 (2019) 113–124.
[13] J. Sun, J. Zhou, S. Liu, Z. Lin, W. Lin, Plume flow field and propulsive performance analysis of a rotating detonation engine, Aerosp. Sci. Technol. 81 (2018) 383–393.
[14] R.A. Gross, Oblique detonation waves, AIAA J. 1 (1963) 1225–1227.
[15] D.T. Pratt, J.W. Humphrey, D.E. Glenn, Morphology of standing oblique detonation waves, J. Propuls. Power 7 (1991) 837–845.
[16] G.P. Menees, H.G. Adelman, J. Cambier, J.V. Bowles, Wave combustors for trans-atmospheric vehicles, J. Propuls. Power 8 (1992) 709–713.
[17] J.M. Powers, D.S. Stewart, Approximate solutions for oblique detonations in the hypersonic limit, AIAA J. 30 (1992) 726–736.
[18] G. Emanuel, D.G. Tuckness, Steady, oblique, detonation waves, Shock Waves 13 (2004) 445–451.
[19] F.K. Lu, H. Fan, D.R. Wilson, Detonation waves induced by a confined wedge, Aerosp. Sci. Technol. 10 (2006) 679–685.
[20] C. Li, K. Kailasanath, E.S. Oran, Detonation structures behind oblique shocks, Phys. Fluids 6 (1993) 1600–1611.
[21] C. Viguier, L.F.F.D. Silva, D. Desbordes, Onset of oblique detonation waves: comparison between experimental and numerical results for hydrogen-air mixtures, Symp., Int., Combust. 26 (1996) 3023–3031.
[22] J.C. Broda, An Experimental Study of Oblique Detonation Waves, University of Connecticut, Connecticut, 1993.
[23] V.V. Vlasenko, V.A. Sabelnikov, Numerical simulation of inviscid flows with hydrogen combustion behind shock waves and in detonation waves, Combust. Explos. Shock Waves 31 (1995) 376–389.
[24] L.F.F.D. Silva, B. Deshaies, Stabilization of an oblique detonation wave by a wedge: a parametric numerical study, Combust. Flame 121 (2000) 152–166.
[25] J. Verreault, A.J. Higgins, R.A. Stowe, Formation and structure of steady oblique and conical detonation waves, AIAA J. 50 (2012) 1766–1772.
[26] H.H. Teng, Z.L. Jiang, On the transition pattern of the oblique detonation structure, J. Fluid Mech. 713 (2012) 659–669.
[27] H. Teng, H.D. Ng, Z. Jiang, Initiation characteristics of wedge-induced oblique detonation waves in a stoichiometric hydrogen-air mixture, Proc. Combust. Inst. 36 (2017) 2735–2742.
[28] S.K. Miao, J. Zhou, Z.Y. Lin, X.D. Cai, S.J. Liu, Numerical study on thermodynamic efficiency and stability of oblique detonation waves, AIAA J. 56 (2018) 3112–3122.
[29] M. Yu, S. Miao, Initiation characteristics of oblique detonation waves in turbulence flows, Acta Astronaut. 147 (2018) 195–204.
[30] S. Bhattrai, H. Tang, Formation of near-Chapman–Jouguet oblique detonation wave over a dual-angle ramp, Aerosp. Sci. Technol. 63 (2017) 1–8.
[31] T. Wang, Y. Zhang, H. Teng, Z. Jiang, H.D. Ng, Numerical study of oblique detonation wave initiation in a stoichiometric hydrogen–air mixture, Phys. Fluids 27 (2015) 096.
[32] P. Yang, H.D. Ng, H. Teng, Z. Jiang, Initiation structure of oblique detonation waves behind conical shocks, Phys. Fluids 29 (2017) 086.
[33] M.V. Papalexandris, A numerical study of wedge-induced detonations, Combust. Flame 120 (2000) 526–538.
[34] J.Y. Choi, D.W. Kim, I.S. Jeung, F. Ma, V. Yang, Cell-like structure of unstable oblique detonation wave from high-resolution numerical simulation, Proc. Combust. Inst. 31 (2007) 2473–2480.
[35] J. Verreault, A.J. Higgins, R.A. Stowe, Formation of transverse waves in oblique detonations, Proc. Combust. Inst. 34 (2013) 1913–1920.
[36] H.H. Teng, Z.L. Jiang, H.D. Ng, Numerical study on unstable surfaces of oblique detonations, J. Fluid Mech. 744 (2014) 111–128.
[37] H. Teng, H.D. Ng, K. Li, C. Luo, Z. Jiang, Evolution of cellular structures on oblique detonation surfaces, Combust. Flame 162 (2015) 470–477.
[38] P. Yang, H. Teng, Z. Jiang, H.D. Ng, Effects of inflow Mach number on oblique detonation initiation with a two-step induction-reaction kinetic model, Combust. Flame 193 (2018) 246–256.
[39] P. Yang, H. Teng, H.D. Ng, Z. Jiang, A numerical study on the instability of oblique detonation waves with a two-step induction-reaction kinetic model, Proc. Combust. Inst. 37 (2019) 3537–3544.
[40] Y. Zhang, L. Zhou, J. Gong, H.D. Ng, H. Teng, Effects of activation energy on the instability of oblique detonation surfaces with a one-step chemistry model, Phys. Fluids 30 (2018) 106–110.
[41] X. Deng, B. Xie, F. Xiao, H. Teng, New accurate and efficient method for stiff detonation capturing, AIAA J. 56 (2018) 4024–4038.
[42] X. Deng, B. Xie, R. Loubère, Y.Y. Shimizu, F. Xiao, Limiter-free discontinuity-capturing scheme for compressible gas dynamics with reactive fronts, Comput. Fluids 171 (2018) 1–14.
[43] J.H. Wang, S. Pan, X.Y. Hu, N.A. Adams, Partial characteristic decomposition for multi-species Euler equations, Comput. Fluids 181 (2019) 364–382.
[44] X. Deng, Z.H. Jiang, F. Xiao, C. Yan, Implicit large eddy simulation of compressible turbulence flow with PnTm BVD scheme, Appl. Math. Model. 77 (2020) 17–31.
[45] Y. Zhang, L. Zhou, H. Meng, H. Teng, Reconstructing wave surface of gaseous detonation based on artificial neural network and proper orthogonal decomposition, Combust. Flame 212 (2020) 156–164.
[46] Y. Liu, X.D. Han, S.B. Yao, J.P. Wang, A numerical investigation of the prompt oblique detonation wave sustained by a finite-length wedge, Shock Waves 26 (2016) 729–739.
[47] B. Bomjan, S. Bhattrai, H. Tang, Characterization of induction and transition methods of oblique detonation waves over dual-angle wedge, Aerosp. Sci. Technol. 82–83 (2018) 394–401.

[48] Y. Fang, Z. Hu, H. Teng, Numerical investigation of oblique detonations induced by a finite wedge in a stoichiometric hydrogen-air mixture, Fuel 234 (2018) 502–507.
[49] K. Iwata, S. Nakaya, M. Tsue, Wedge-stabilized oblique detonation in an inhomogeneous hydrogen–air mixture, Proc. Combust. Inst. 36 (2017) 2761–2769.
[50] Y. Fang, Z. Hu, H. Teng, Z. Jiang, H.D. Ng, Numerical study of inflow equivalence ratio inhomogeneity on oblique detonation formation in hydrogen-air mixtures, Aerosp. Sci. Technol. 71 (2017) 256–263.
[51] Y. Liu, L. Wang, B.G. Xiao, Z.H. Yan, C. Wang, Hysteresis phenomenon of the oblique detonation wave, Combust. Flame 192 (2018) 170–179.
[52] Y. Zhang, P. Yang, H. Teng, H.D. Ng, C. Wen, Transition between different initiation structures of wedge-induced oblique detonations, AIAA J. 56 (2018) 4016–4023.
[53] P. Yang, H.D. Ng, H. Teng, Numerical study of wedge-induced oblique detonations in unsteady flow, J. Fluid Mech. 876 (2019) 264–287.
[54] C. Li, K. Kailasanath, E.S. Oran, Effects of boundary layers on oblique-detonation structures, in: Aerospace Sciences Meeting, 2013.
[55] A.F. Wang, W. Zhao, Z.L. Jiang, The criterion of the existence or in existence of transverse shock wave at wedge supported oblique detonation wave, Acta Mech. Sin. 27 (2011) 611–619.
[56] V.N. Gamezo, D. Desbordes, E.S. Oran, Formation and evolution of two-dimensional cellular detonations, Combust. Flame 116 (1999) 154–165.
[57] V.N. Gamezo, D. Desbordes, E.S. Oran, Two-dimensional reactive flow dynamics in cellular detonation waves, Shock Waves 9 (1999) 11–17.
[58] K. Mazaheri, Y. Mahmoudi, M.I. Radulescu, Diffusion and hydrodynamic instabilities in gaseous detonations, Combust. Flame 159 (2012) 2138–2154.
[59] M.P. Burke, M. Chaos, Y. Ju, F.L. Dryer, S.L. Klippenstein, Comprehensive H2/O2 kinetic model for high-pressure combustion, Int. J. Chem. Kinet. 44 (2012) 444–474.
[60] R.J. Kee, F.M. Rupley, E. Meeks, J.A. Miller, Chemkin-II: a Fortran chemical kinetics package for the analysis of gas-phase chemical and plasma kinetics, Sandia National Laboratories, UC-405, SAND96-8216, 1989.